

Simulation study of reversible random sequential adsorption of lattice animals on a three-dimensional cubic lattice

Julija R. Šćepanović ^a, Danica Stojiljković ^{a,*}, Zorica M. Jakšić ^a,
Ljuba Budinski-Petković ^b, Slobodan B. Vrhovac ^a

^a Institute of Physics Belgrade, University of Belgrade, Pregrevica 118, Zemun Belgrade, 11080, Serbia

^b Faculty of Technical Sciences, University of Novi Sad, Trg D. Obradovića 6, Novi Sad, 21000, Serbia

ARTICLE INFO

Keywords:

Random sequential adsorption
Desorption
Three-dimensional (3D) lattice
Lattice animals

ABSTRACT

The properties of the reversible Random Sequential Adsorption (RSA) of objects of various shapes on a simple three-dimensional (3D) cubic lattice are studied numerically using Monte Carlo simulations. Depositing objects are “lattice animals” made of a certain number of nearest-neighbor sites on a lattice. This work aims to investigate the impact of the geometrical properties of shapes on the temporal evolution of the density $\theta(t)$. We analyzed all lattice animals of size $n = 1, 2, 3$, and 4. The approach of the density $\theta(t)$ to the equilibrium density θ_∞ is found to be stretched exponential, $\theta_\infty - \theta(t) \sim \exp(-(t/\tau)^\beta)$, for all lattice animals. The characteristic time scale τ was found to decrease with the probability of desorption P_{des} according to the power law, $\tau = A(P_{\text{des}})^{-\gamma}$. The exponent γ remains unchanged in all shapes of the same size. The parameter A changes depending on the number of different orientations m that the lattice animals can take when placed on a cubic lattice. Orientations of the lattice animal deposited in two randomly chosen places on the lattice are different if one of them cannot be translated into the other. Our findings indicate that the deposition dynamics slows significantly as m decreases. Furthermore, for objects of the same size, the value of parameter β increases with the number of possible orientations m of the shape. The structural heterogeneity in the local relaxation dynamics gives rise to a stretched exponential behavior of the density $\theta(t)$ with a lower value of β .

1. Introduction

The problem of packing non-overlapping particles has long intrigued researchers in the fields of discrete mathematics, geometry, and physics [1,2]. One of the primary goals is to uncover the organizing principles that lead to the densest packing of various objects [3]. The interplay of various controlling parameters, such as the geometric shapes and material properties of the particles, the influence of gravitational forces, and different methods employed for packing, plays an important role in the arrangement of particles. The comprehensive model that reliably predicts the arrangement of packed particles is missing, and the packing of particles is still far from well understood. This insight is key to explaining numerous natural phenomena that occur in the liquid, glassy and crystalline states of matter [4–6], heterogeneous materials [5], crystalline polymers [7], and biological systems [8,9]. Hence, the need to develop more advanced predictive models in this field arises.

* Corresponding author.

E-mail address: danica@ipb.ac.rs (D. Stojiljković).

<https://doi.org/10.1016/j.cjph.2025.12.010>

Received 2 September 2025; Received in revised form 20 November 2025; Accepted 8 December 2025

Available online 11 December 2025

0577-9073/© 2025 The Physical Society of the Republic of China (Taiwan). Published by Elsevier B.V. All rights are reserved, including those for text and data mining, AI training, and similar technologies.

The random sequential adsorption (RSA) method uses a simple, non-trivial model in which the effects of excluded volume are most dominant. This model proved to be effective for studying the packing of objects of various shapes [10], the structure of low-temperature phases of matter, and particle aggregation and jamming in a wide variety of systems: from granular media [11,12] to heterogeneous materials [13–15] and biological systems [16,17]. The RSA model attempts sequential additions of hard particles at randomly chosen locations within an n -dimensional volume [18]. A trial particle is added to the configuration if it does not overlap with any of the previously placed particles. Each accepted particle further reduces the substrate space available for new particles and affects the geometry of all subsequent placements. The time evolution of the density of the system, $\theta(t)$, describes the kinetic properties of the deposition process. The density $\theta(t)$ increases steadily and approaches the jamming threshold θ_J over time, at which point no more particles can be accommodated.

Most research focuses on random close packings (RCPs), where neighboring particles are in contact with each other [2]. The introduction of the order can lead to higher packing densities [19]. RCP state is challenging to define because the properties of RCPs are highly sensitive to the numerical protocol used to pack the objects [20]. In contrast, for RSA packing, the jammed state and the asymptotic packing density are clearly defined, making it more convenient to study how object shape influences the structure and density of the packing. However, the RSA model proposes depositions of 3D objects in locations surrounded by previously deposited objects, which is not physically feasible.

The adsorption of particles is usually accompanied by desorption [11,12,21–23]. Desorption makes the process reversible and allows the system to reach an equilibrium state in which the adsorption and desorption rates balance out. The equilibrium density θ_∞ is higher than the maximum density achieved without desorption θ_J . The ratio of the adsorption rate to the desorption rate $K = k_+/k_-$ governs the kinetics of reversible RSA. When K is large, the system quickly reaches a density $\theta \simeq \theta_J$, then gradually relaxes towards an equilibrium value θ_∞ [24–26]. An adsorption-desorption model qualitatively reproduces the slow relaxation of density [11,25,27], the memory effects [12,28], and other characteristics of weakly vibrated granular materials.

In Refs. [29–31] we have carried out extensive numerical simulations of the random deposition of large collections of objects known as lattice animals on a simple 3D cubic lattice. A lattice animal presents a set of connected lattice sites: each site in the set is the nearest neighbor of at least one other site in the set. The size of a lattice animal is the number n of sites in a set. We have found that the symmetry of a lattice animal exerts a decisive influence on adsorption kinetics near the jamming limit θ_J . For binary mixtures [30,31], the approach rate to the jamming limit is governed by the less symmetric component. Depending on the local geometry of the components of a mixture, the jamming density of the mixture can be greater than one or both single-component jamming densities. The second case is more common, while in the first case, the jamming density of the mixture is very close to the higher single-component jamming density.

Recently, we have studied numerically the percolation properties of the RSA of lattice animals on a simple three-dimensional cubic lattice [32]. We found that the number of nearest neighbors N_1 and the radius of gyration R_g of the objects are correlated with the values of the percolation threshold θ_p^* . For objects of identical size, the percolation threshold θ_p^* decreases as the number of object's nearest neighbors increases. If objects have the same size and the same number of nearest neighbors N_1 , their percolation threshold θ_p^* decreases with increasing radius of gyration R_g .

Irreversible deposition in three dimensions has been studied numerically for packings built of spheres [18,33–35], uniaxial ellipsoids [36], dimers [37], cubes and cuboids [38,39]. In this paper, we present the results of Monte Carlo simulations for the reversible RSA of lattice animals on a 3D cubic lattice. The number of lattice animals examined provides a solid foundation for exploring how the geometrical properties of these shapes influence jamming density θ_J and the temporal evolution of density $\theta(t)$. Reversible deposition of lattice animals on 3D lattices is a complex issue, making it challenging to develop even a qualitative understanding of how shape affects packing density and process dynamics. Various factors, such as desorption probability, size, and symmetry of the shapes, contribute to a diverse range of behaviors. Our aim is to show that only one function can be used to describe the growth of the coverage in the whole range above the jamming limit. Here, we confirm that over the jamming density, up to the equilibrium coverage, desorption-mediated filling of the cubic lattice by extended objects proceeds via the stretched-exponential law. Additionally, it will be discussed how the symmetry properties of the extended objects in the reversible RSA model are related to the dissipative properties of the grains during vibratory compaction of granular materials.

The paper is organized as follows. Section 2 describes the details of the simulations. We give the simulation results and discussions in Section 3. Section 4 contains some additional comments and final remarks.

2. Definition of the model and the simulation method

In 3D Euclidean space, the cubic lattice \mathbb{Z}^3 can be represented as the space-filling set of unit cubes or the set of lattice vertices that are one unit apart (\mathbb{Z} denotes the set of integers). In the first representation, polycubes of size n are defined as a set of n connected cubes. Two cubes are connected if they share a common face. Similarly, in the second representation, lattice animals of size n are defined as a set of n connected lattice sites: each element of a set is a nearest neighbor of at least one other site in the set. Due to the self-dual nature of the cubic lattice, polycubes are equivalent to site animals on the dual lattice. As a result, the count of polycubes with n cells exactly matches the count of 3D lattice animals with n vertices. This can be generalized to an N -dimensional space. In this work, we will use the terms “lattice animal” and “polycube” interchangeably as we investigate the reversible RSA deposition of these objects on a 3D cubic lattice.

Lattice animals can be regarded as *fixed* or *free*. Fixed animals are considered distinct if they have different shapes or orientations; in other words, two fixed animals are identical if one can be transformed into the other through translation. Free animals are defined solely by their shape and not their orientation.

Polycubes are often discussed in the context of simple combinatorial problems, particularly enumeration. Enumeration involves determining the number of polycubes that correspond to a specific parameter, usually their size or perimeter. The number of fixed d -dimensional polycubes of size n is typically denoted by $A_d(n)$ in the literature, while the number of free d -dimensional polycubes of size n with m different orientations is denoted as $A_d^m(n)$. Lunnon [40] was the first to successfully enumerate animals on a 2D square lattice (polyominoes), computing their number up to size 18, although he made a slight error in $A_2(17)$. He also analyzed three-dimensional polycubes by examining symmetry groups and manually computed $A_3(n)$ for sizes up to $n = 6$ [41]. Interestingly, to this day, there is no known analytic formula for $A_d(n)$ when $d > 1$. The only recognized methods for calculating $A_d(n)$ rely on explicitly or implicitly enumerating all polyominoes or polycubes using various numerical algorithms [40,42–45].

Although most polycubes are asymmetric, many exhibit more complex symmetry groups. The achiral octahedral group, O_h , is the full symmetry group of the cube or octahedron in a three-dimensional space, including rotations and reflections. It is the symmetry group of the cubic lattice and has 48 elements. It consists of all isometries (rotations, reflections, and their combinations) that map a cube or octahedron onto itself. Lunnon [41] found that O_h has 98 subgroups divided into 33 conjugacy sets, which represent different types of polycube symmetry.

The chiral octahedral O group is a subgroup of O_h that excludes reflections and has 24 elements. Reflections are improper transformations: no physical motion can transform an asymmetric object into its mirror image. Polycubes and their mirror pairs, also known as chiral twins, are regarded distinct. Free polycubes can have $m \in \{1, 3, 4, 6, 8, 12, 24\}$ different orientations on the simple cubic lattice [46], depending on their symmetry. Since we exclusively consider free lattice animals in this work, we will omit the term “free” in the following text.

Table 1 provides a list of all polycubes of sizes $n = 1, 2, 3$, and 4 along with the number of distinct orientations m for each object. Polycubes of sizes $n = 1, 2$, and 3 are planar and can have up to twelve orientations (as represented by the object V3). There are eight tetracubes, of which five are planar [46]. An example of chiral twins is a pair of tetracubes labeled A4 and its mirror image, B4.

The numerical values of the jamming densities θ_j for all lattice animals of size $n \leq 4$ are provided in Table 1. For objects of size $n \leq 3$, the jamming density θ_j is greater than approximately 0.84. In contrast, for all objects of size $n = 4$, θ_j falls within the interval of 0.78 to 0.84. This trend indicates that the jamming densities θ_j decrease as the size n of the objects increases. The decline in jamming density θ_j is directly the result of increased frustration in spatial adsorption. As expected, each chiral pair exhibits identical values of jamming density.

2.1. Simulation method

The numerical algorithm for depositing a lattice animal in a randomly selected location on the three-dimensional substrate was detailed in the previous paper [29]. In this section, we will provide a brief overview of the algorithm, including the necessary additions for the random desorption of objects.

The adsorption and desorption processes are statistically independent and occur sequentially, each with specific probabilities. At each Monte Carlo step, an adsorption attempt is made with probability P_a and a desorption attempt with probability P_{des} . The kinetics of these adsorption-desorption processes is determined by the ratio of desorption to adsorption probability P_{des}/P_a [23,24,26]. Since our focus is on the ratio P_{des}/P_a , we can simplify the process to save computer time by setting the adsorption probability $P_a = 1$. For each of these processes, a lattice site is selected randomly.


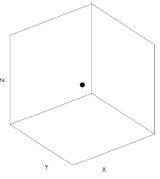

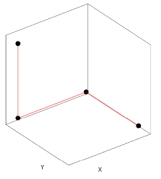

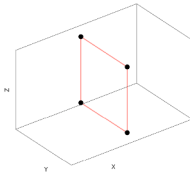

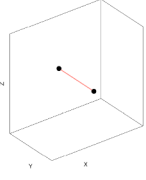

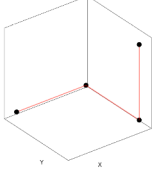

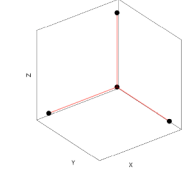

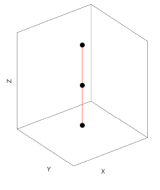

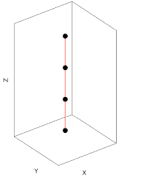

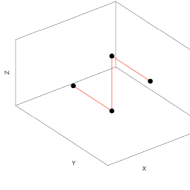

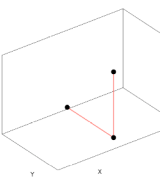

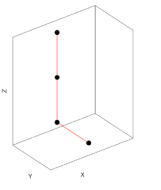

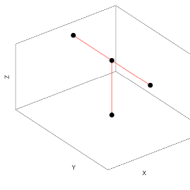
The random deposition of lattice animals was performed as follows. We define a primary lattice animal as a connected set of sites in the cubic lattice that contains the origin ($x = 0, y = 0, z = 0$). We refer to that point as the head of an object. At each Monte Carlo step, a lattice site is selected at random. If the selected site is unoccupied, the deposition of the chosen object is attempted in one of the 24 orientations, which is selected at random. Then, we fix the head of the object at the selected site and check whether all necessary sites are unoccupied. If so, we occupy these sites, thus placing the object. Otherwise, we reject the deposition trial. The numerical algorithm that searches for all possible object orientations and selects the random orientation of a lattice animal is presented in the previous paper [29]. The randomly oriented object is generated by consecutively rotating the primary object around all three principal axes of the lattice at randomly chosen angles $\psi \in \{0, \pi/2, \pi, 3\pi/2\}$. However, due to the non-commutativity of rotation operators in 3D [47], the order of these rotations must also be chosen randomly [29].

Each adsorption attempt is followed by a desorption attempt, which occurs with a probability P_{des} . The desorption process begins by randomly selecting a lattice site. If the chosen site is unoccupied by the head of a previously deposited object, the desorption step fails, and the process continues by selecting another site for an adsorption attempt. Conversely, if the selected site is occupied by the head of deposited object, that object is removed from the lattice. We have confirmed that the use of different heads for all examined objects yields quantitatively the same results for the temporal evolution of density $\theta(t)$. Desorption of objects can also be achieved in another way. In the case where an object is desorbed when any node belonging to the object is randomly selected, the probability of desorption P_{des} increases by a factor equal to the number of nodes the object covers. We have opted for the previously described algorithm, since it enables easier comparison of results for objects of different sizes and allows an easier code development in the case of mixtures of various lattice shapes.

During the simulation, we record the number of lattice sites that are considered inaccessible. Inaccessible sites include both those that are already occupied and those that, while unoccupied, cannot serve as the head position for depositing the object in any of the 24 possible orientations, due to spatial constraints from neighboring sites. The jamming limit is reached when all sites in the lattice become inaccessible [29]. The system is then jammed in a non-equilibrium disordered state. When the deposited particles are subjected to desorption, the system formed by the adsorbed objects on the lattice can reach an equilibrium state. In the reversible

Table 1

Shown here are all polycubes of size $n = 1, 2, 3, 4$ together with the equivalent lattice animals (x) on the dual lattice. For each lattice animal (x) with m possible orientations, $\theta_J^{(x)}$ is the jamming density [29]. The numbers in parentheses are the numerical values of the standard uncertainty of $\theta_J^{(x)}$ referred to the last digits of the quoted values.

$(x), m; \theta_J^{(x)}$	$(x), m; \theta_J^{(x)}$	$(x), m; \theta_J^{(x)}$
  (M),1; 1.0000(0)	  (A4),12; 0.8178(2)	  (O4),3; 0.8079(3)
  (D),3; 0.9184(1)	  (B4),12; 0.8178(2)	  (P4),8; 0.7941(3)
  (I3),3; 0.8390(2)	  (I4),3; 0.7808(3)	  (S4),12; 0.8149(2)
  (V3),12; 0.8788(2)	  (L4),24; 0.8339(2)	  (T4),12; 0.8114(3)

case, the process reaches a steady state in which the rate of desorption exactly balances the rate of adsorption. In this paper, θ_∞ will designate the steady state value of the density.

Correlations in RSA are known to decay extremely fast [48–50]. Therefore, one can obtain high-precision results numerically on relatively small lattices, without worrying about finite-size effects and averaging over not too many runs because the system is self-averaging. Numerical studies have shown that the finite-size effects on the lattice of size L can be neglected for object sizes $< L/8$ [30,51]. Consequently, Monte Carlo simulations are performed on a triangular lattice of size $L = 64$. Periodic boundary conditions are used in all directions. The time is counted by the number of attempts to select a lattice site and scaled by the total number of lattice sites $L^3 \approx 2.6 \times 10^5$. Data are averaged over 128 independent runs for each choice of lattice animal and each desorption probability P_{des} .

3. Results and discussion

Using the reversible RSA algorithm defined in the previous section, extensive calculations were performed to determine the time evolution of the density $\theta(t)$ of lattice animals deposited on the lattice. The dynamics of the reversible deposition process were analyzed for all objects listed in Table 1. It should be noted that the results for objects A4 and B4 are identical because they form a chiral pair.

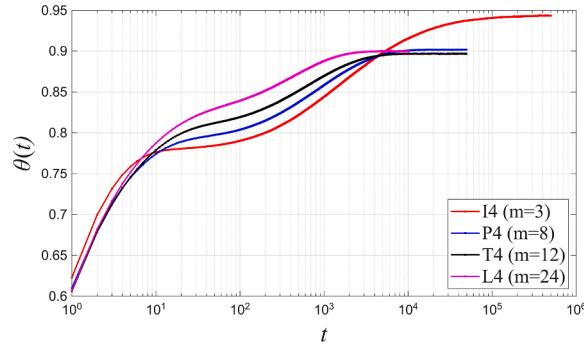


Fig. 1. Temporal evolution of density $\theta(t)$ is for lattice animals I4, P4, T4, and L4 of size $n = 4$ in the case of desorption probability $P_{\text{des}} = 0.001$. The number of possible orientations $m = 3, 8, 12, 24$ for these objects is given in the legend.

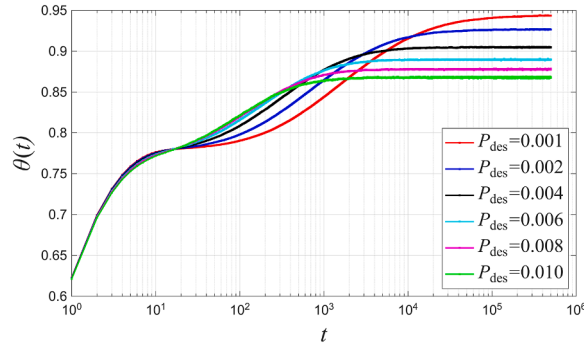


Fig. 2. Temporal behavior of the density $\theta(t)$ of object I4 for various values of desorption probabilities P_{des} , as indicated in the legend. The equilibrium density θ_{∞} is found to decrease with the desorption probability P_{des} . Error bars representing the standard deviation are omitted from the figure since their magnitude is less than the width of the plotted lines.

Simulations of adsorption-desorption processes were performed for a wide range of desorption probabilities $P_{\text{des}} = 0.001 - 0.010$. We investigate the role that the symmetry properties of the shapes play in the deposition process.

In Fig. 1, the temporal evolution of the density $\theta(t)$ is shown for objects I4, P4, T4 and L4, which have all four possible orientation numbers $m = 3, 8, 12, 24$ for lattice animals of size $n = 4$. Here, we consider the case of rapid adsorption and slow desorption $P_{\text{des}}/P_a = 0.001 \ll 1$. Then, the relaxation of the system to its equilibrium density θ_{∞} is a two-stage process. In the early stages of the process, when the density is small, the adsorption process is dominant, and the density grows rapidly over time, displaying an RSA-like behavior. For densities large enough ($\theta(t) > \theta_J$), the growth of the density $\theta(t)$ requires the rearrangement of the increasing number of particles to open a hole large enough for the insertion of an additional particle. Therefore, with increasing density, the desorption process becomes increasingly important. This strongly suggests that collective events are responsible for the evolution of $\theta(t)$ for $\theta(t) > \theta_J$. Because these events involve multiple particle transitions, they occur on a longer timescale than simple adsorption/desorption events at low densities. We are interested in the time evolution of the density $\theta(t)$ in this later post-jamming time range. The results shown in Fig. 1 suggest that for objects with a smaller number of possible orientations m , the density $\theta(t)$ reaches its equilibrium value θ_{∞} more slowly. The kinetics of these processes will be explained and quantitatively characterized later.

Fig. 2 shows the time dependence of the density $\theta(t)$ resulting from the reversible RSA of the I4 shape for various values of P_{des} . It is observed that a higher value for the equilibrium density θ_{∞} is reached for the lower value of the desorption probability P_{des} . In fact, the density at which a balance is established between the rates at which objects are deposited onto the grid and removed from it increases as the probability of desorption decreases. In other words, when the desorption probability is low, the system density must reach a sufficiently high level for the rates of deposited and desorbed particles to equalize. Consequently, as the desorption probability decreases, the value of the equilibrium density increases.

We have attempted to fit various functional forms to the simulation data obtained, with a particular focus on the relaxation functions proposed in experimental and numerical studies of disordered systems [52]. We find that the stretched exponential relaxation of the form

$$\theta(t) = \theta_{\infty} - \Delta\theta \exp\left(-(t/\tau)^{\beta}\right) \quad (1)$$

accurately describes the approach to the equilibrium state. Note that the parameters $\Delta\theta$, the relaxation time τ , and the stretching exponent β are the fitting parameters. For a given object, the values of the steady state density θ_{∞} , the parameter $\Delta\theta$, and the relaxation time τ depend on the desorption probability P_{des} .

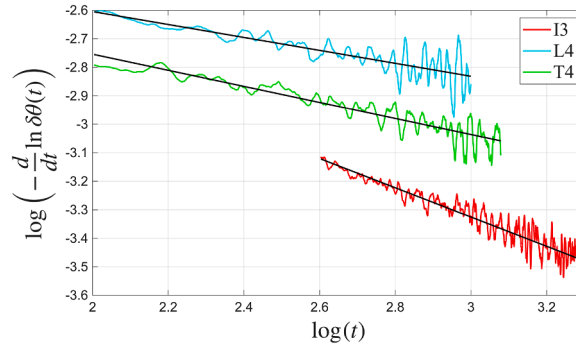


Fig. 3. Test for the presence of the stretched exponential law (1) in the time dependence of density $\theta(t)$ for lattice animals I3, L4, and T4, as indicated in the legend. Straight line sections of the curves show where the law holds. The black straight lines are power-law fits of Eq. (5). All the results are for $P_{\text{des}} = 0.001$.

To confirm the validity of the stretched exponential behavior of the density $\theta(t)$, the following procedure was applied. The function (1) can be written as

$$\delta\theta(t) = \Delta\theta \exp\left(-\left(t/\tau\right)^\beta\right), \quad (2)$$

where $\delta\theta = \theta_\infty - \theta(t)$. Differentiating Eq. (2) by time, we get

$$\frac{d\delta\theta(t)}{dt} = -\Delta\theta \exp\left(-\left(t/\tau\right)^\beta\right) \frac{\beta}{\tau} \left(\frac{t}{\tau}\right)^{\beta-1}. \quad (3)$$

Eq. (3) can be written in the form

$$-\frac{1}{\delta\theta(t)} \frac{d\delta\theta(t)}{dt} = \frac{\beta}{\tau^\beta} t^{\beta-1}. \quad (4)$$

From Eq. (4), it follows that

$$-\frac{d}{dt} [\ln(\delta\theta(t))] = \frac{\beta}{\tau^\beta} t^{\beta-1}, \quad (5)$$

which means that a double logarithmic plot of the time derivative of $\ln(\delta\theta(t))$ versus time t is a straight line in the case of the stretched exponential function (1).

From Eq. (5) it follows

$$\log_{10}\left(-\frac{d}{dt} \ln(\delta\theta)\right) = (\beta - 1) \log_{10} t + \log_{10}\left(\frac{\beta}{\tau^\beta}\right). \quad (6)$$

Eq. (6) has the linear form $y = kx + m$, where $x = \log_{10} t$, $y = \log_{10}(-\frac{d}{dt} \ln(\delta\theta))$, and

$$k = \beta - 1, \quad m = \log_{10}\left(\frac{\beta}{\tau^\beta}\right). \quad (7)$$

By fitting the dependence (6) with a linear function $y = kx + m$, we determine the fit coefficients k and m , from which we obtain the parameters:

$$\beta = k + 1, \quad \tau = \left(\frac{\beta}{10^m}\right)^{1/\beta} = \left(\frac{k+1}{10^m}\right)^{1/(k+1)}. \quad (8)$$

The time derivatives of $\ln(\delta\theta(t))$ were calculated numerically from the simulation data. Representative examples of the double logarithmic plots of $-d[\ln(\delta\theta(t))]/dt$ are presented in Fig. 3, for objects I3, L4 and T4 (Table 1), and for the probability of desorption $P_{\text{des}} = 0.001$. These plots reveal that the curves are straight lines in the post-jamming time range ($\theta(t) > \theta_j$). The same holds for all tested values of desorption probabilities ($P_{\text{des}} = 0.001 - 0.010$). This suggests that the relaxation of the density $\theta(t)$ above the jamming limit towards the equilibrium value θ_∞ can be described by a stretched exponential function of the form (1). The fitting parameters β and τ are obtained from the power-law fit described in Eq. (5). The fitting values for the parameter $\Delta\theta$ are determined for each pair (τ, β) using the least squares method.

The plots of the simulation data and the corresponding stretched exponential fitting functions (Eq. (1)) are given in Fig. 4 for lattice animals I3, L4 and T4, and for the probability of desorption $P_{\text{des}} = 0.001$. The fitting parameters τ , β , and $\Delta\theta$ were obtained as previously described. The stretched exponential fitting function shows an excellent agreement with the simulation results in the region above the jamming density. It should be noted that in this region the stretched exponential fits (1) of the simulation data give very high correlation coefficients ($\gtrsim 0.97$). Furthermore, we analyzed the time evolution of the density $\theta(t)$ in the range above the jamming limit by employing a nonlinear fitting procedure that utilized the Nelder-Mead simplex algorithm [53] to minimize a nonlinear function with multiple variables. We verified that both fit procedures give similar correlation coefficients and yield nearly

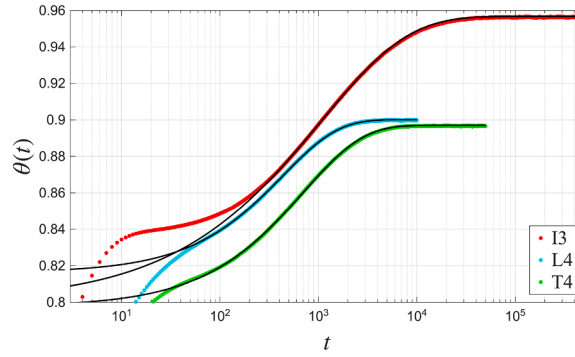


Fig. 4. Temporal behavior of the density $\theta(t)$ for reversible deposition of lattice animals I3, L4, and T4, as indicated in the legend. The continuous black curves are the stretched exponential fits of Eq. (1). All the results are for $P_{\text{des}} = 0.001$.

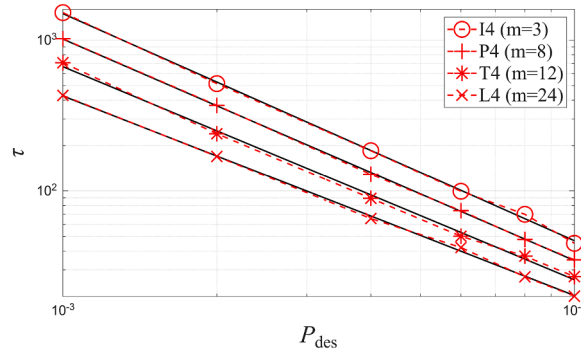


Fig. 5. Parameter τ of the stretched exponential fit (Eq. (1)) vs desorption probability P_{des} for lattice animals I4, P4, T4 and L4 of size $n = 4$ (see, Table 1), but various number of possible orientations $m \in \{3, 8, 12, 24\}$, as indicated in the legend. The black solid lines are the power-law fits of Eq. (9), with the same exponent $\gamma = 1.42 \pm 0.07$ for all the shapes.

identical results for the parameters τ and β . Since the first procedure is more straightforward to implement, we systematically used it for the analysis of the results.

To better understand the effects of the shape of the object on the kinetics of reversible RSA, we closely examined how the fitting parameters τ and β depend on the desorption probability P_{des} . Data for τ vs P_{des} for lattice animals I4, P4, T4 and L4 of size $n = 4$, but various numbers of possible orientations $m \in \{3, 8, 12, 24\}$ are plotted in Fig. 5. It is remarkable that for a given lattice animal, the parameter τ appears to be a simple power law of the desorption probability P_{des} :

$$\tau = A (P_{\text{des}})^{-\gamma}, \quad (9)$$

with the same exponent $\gamma = 1.42 \pm 0.07$ for all shapes. As shown in Fig. 5, more symmetric shapes (lower values of m) exhibit larger values of the relaxation time τ for a given desorption probability P_{des} . This indicates that the deposition dynamics becomes significantly slower as m decreases.

It is important to understand why the deposition dynamics slows as the number of possible orientations m of the shape decreases. First, we will discuss the mechanisms that govern the dynamics of the reversible deposition process. We will focus on the case of weak desorption (that is, low values of P_{des}), where the system of adsorbed particles continuously evolves toward an equilibrium disordered state. When the value of θ_j is reached, rare desorption events are typically followed by immediate readsorption. These single-particle events do not change the total number of particles. In essence, it is the collective events that drive the evolution of the density θ above the jamming limit θ_j [23,54]. The transition from a state with $\theta > \theta_j$ to its steady-state value θ_∞ is mainly influenced by two types of two-particle processes. In the first process, referred to as “2 → 1”, the number of deposited objects decreases by one. This occurs when two adjacent objects leave and one object takes their place. The opposite process, known as “1 → 2”, results in the addition of an extra object to the lattice: one object exits, creating a void large enough for two objects to fit. The rate of the “2 → 1” process has three contributing factors. First, an object must leave the lattice. Next, an adjacent object must leave before the hole created by the first object is filled. Finally, this larger hole must be blocked by a poorly placed object. Conversely, in the “1 → 2” process, the void left by the outgoing object must be large enough to accommodate two objects. It is important to note that the first incoming object must be positioned with sufficient precision to leave enough space for the second object.

It is clear that the process “1 → 2” has an overall rate that is proportional to $P_{\text{des}} < 1$. In contrast, the process “2 → 1” involves two consecutive desorption events, which makes it reasonable to assume that its overall rate is proportional to $(P_{\text{des}})^2$, which is also less than $P_{\text{des}} < 1$. This is the primary reason why for densities that are not close to the steady-state value, the collective event “1 → 2”

occurs more frequently than the reverse event “2 → 1”. This phenomenon continues until the density approaches the equilibrium value. As the density $\theta(t)$ increases, the available space for deposition decreases. Consequently, the overall rate at which density increases gradually diminishes. The efficiency of desorption relative to adsorption increases, leading the system to a steady state where the rate of the “2 → 1” process is balanced by the rate of the “1 → 2” process.

Now, we try to explain how the symmetry of the shape changes the dynamics of the collective processes. Let us first explain the correspondence that exists between the symmetry of shapes and the number of their different orientations. The symmetry of a lattice animal refers to the group of all isometries (rotations, reflections, etc.) that map the animal onto itself. This is described by its symmetry group S , a subgroup of the cubic lattice symmetry group O_h . The achiral octahedral group O_h with 48 elements is the ambient symmetry group (including proper rotations, reflections, inversion, and rotor-flections). The number of distinct orientations of a free lattice animal m is the number of orbits of the animal under the action of the lattice’s symmetry group O_h (Burnside’s Lemma [55]):

$$m = \frac{|O_h|}{|S|} = \frac{48}{|S|}, \quad (10)$$

where $|S|$ is the order of the animal’s symmetry group. In our case, when only rotations are considered (excluding 24 improper transformations), the symmetry group O_h is replaced by the rotational subgroup O (the chiral octahedral group), which has $|O| = 24$. Therefore, the number of distinct orientations m can be calculated as $m = 24/|S|$.

Animals with high symmetry (large $|S|$) have fewer distinct orientations. For example, a fully symmetric animal (e.g. a single site or a cube with all symmetries of O or O_h) has $|S| = 24$, so it has only $m = 24/24 = 1$ orientation. A linear chain of n sites (shapes D, I3 and I4) may have $|S| = 8$ (for example, the symmetry group might be D_{2h}), leading to $m = 24/8 = 3$ orientations. Animals with low symmetry (small $|S|$) have more orientations. For example, asymmetric animal L4 with $|S| = 1$ (symmetry group is a trivial group C_1 ; only identity transformation) has $m = 24/1 = 24$ orientations. An L-shaped animal V3 may have $|S| = 2$ (e.g., symmetry group might be C_2 ; a single π rotation, giving $24/2 = 12$ orientations). Hence, the symmetry of free-lattice animals on a 3D cubic lattice is inversely related to the number of their possible different orientations.

The symmetry properties of lattice animals significantly influence the filling of small, isolated targets on the lattice. There are only a limited number of spatial orientations in which an object can occupy a previously opened location, especially when that location is small. When an object can be placed in an isolated available position on the grid, the probability of selecting an appropriate spatial orientation increases as the symmetry of the object increases. Shapes with higher symmetry are more suitable for optimal placement and interaction within their environments. Consequently, greater symmetry enhances the likelihood of single-particle readsorptions, which do not change the total number of deposited objects on the grid. This increase in symmetry extends the mean waiting time between consecutive two-particle events “1 → 2”, leading to a slowdown in density growth above the jamming density θ_j .

In contrast, asymmetrical shapes have a lower probability of achieving a spatial orientation that allows them to fit into the selected location. Hence, the significant decrease in the probability of single-particle readsorption for the asymmetrical shapes is thus a clear consequence of the enhanced frustration during spatial adsorption. As a consequence, the desorption process effectively creates openings that are large enough to accommodate two or more particles. This reduction in mean waiting time between consecutive multiparticle events “1 → 2” leads to a faster growth rate in density.

Figs. 6 and 7 show the dependence of parameter τ in the stretched exponential fit (Eq. (1)) on the desorption probability P_{des} for lattice animals with $m = 3$ and $m = 12$ possible orientations, respectively. The first notable observation is the collapse of the τ vs P_{des} curves for objects of the same size n and the same number of orientations m . This suggests that the parameter A in the power law (9) is nearly the same for all objects of identical size n that possess the same number of orientations m . For the shapes I4 and O4 (Fig. 6), both having a size of $n = 4$ and an orientation number of $m = 3$, we obtained $A = 0.048 \pm 0.003$. For objects A4, S4 and T4 (Fig. 7), which also have a size $n = 4$ but a larger number of orientations $m = 12$, a slightly lower value $A = 0.037 \pm 0.002$ is obtained. This behavior of the parameter A represents a translation of the curves showing the dependence of parameter τ on P_{des} toward lower values as the number of object orientations m increases, which was previously shown in Fig. 5. Figs. 6 and 7 demonstrate that, for objects with the same number of orientations, the slope of the fit lines (Eq. (9)) decreases slightly with a reduction in object size: $\gamma(I4, P4, T4, L4) = 1.42 \pm 0.07$, $\gamma(I3, V3) = 1.30 \pm 0.02$, and $\gamma(D) = 1.15$. As the size n of the object decreases, the fit parameter τ changes to lower values for a given desorption probability P_{des} . This change indicates that the deposition dynamics become faster with decreasing object size, due to reduced frustration of spatial adsorption.

Previously, we analyzed the behavior of the fit parameter τ , which represents the characteristic relaxation time of the system. It is a time scale that indicates the rate at which the system relaxes toward equilibrium. In the following text, we present the results of the analysis of the behavior of the stretching exponent β . The fitting parameter β in Eq. (1) characterizes the shape of the relaxation function and reflects the complexity or heterogeneity of the relaxation process. Its value typically lies in the range $0 < \beta \leq 1$. When $\beta = 1$, the expression (1) reduces to a simple exponential form, which describes a single homogeneous relaxation process with a single characteristic timescale (Debye relaxation). When $\beta < 1$, the relaxation is “stretched”, indicating a distribution of relaxation times rather than a single timescale. This suggests that the system has a range of relaxation processes that occur simultaneously, often due to disorder, heterogeneity, or cooperative dynamics in complex systems.

The dependence of the fitting parameter β on the desorption probability P_{des} is shown in Fig. 8 for the lattice animals I4, P4, T4 and L4 of the same size $n = 4$, but for various numbers of possible orientations $m \in \{3, 8, 12, 24\}$. The values of the parameter β for all objects and the values of the desorption probability P_{des} are less than one, which indicates a stretched, non-exponential decay due to a distribution of relaxation times. It is evident that the exponent β depends weakly on the probability of desorption. However, its value for objects of the same size increases with the number of possible orientations m of the object. For example, the values of

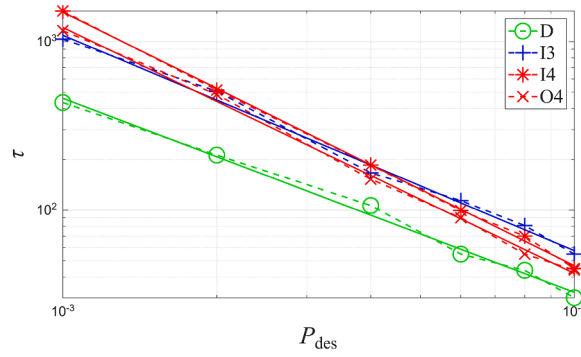


Fig. 6. Parameter τ of the stretched exponential fit (Eq. (1)) vs desorption probability P_{des} for lattice animals D, I3, I4, and O4 with the same number of possible orientations $m = 3$, but various size (see, Table 1). The straight solid lines are the power-law fits of Eq. (9).

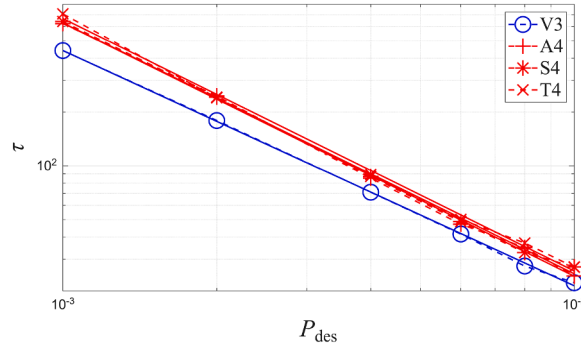


Fig. 7. Parameter τ of the stretched exponential fit (Eq. (1)) vs desorption probability P_{des} for lattice animals V3, A4, S4, and T4 with the same number of possible orientations $m = 12$, but various size (see, Table 1). The straight solid lines are the power-law fits of Eq. (9).

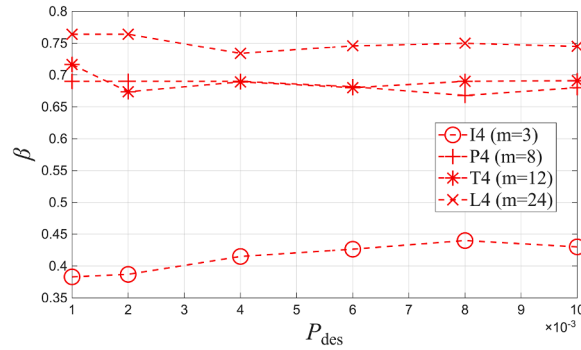


Fig. 8. Parameter β of the stretched exponential fit (Eq. (1)) vs desorption probability P_{des} for lattice animals I4, P4, T4, and L4 of size $n = 4$ (see, Table 1), but various number of possible orientations $m \in \{3, 8, 12, 24\}$, as indicated in the legend.

the parameter β for the L4 object ($m = 24$) are significantly higher than those for the I4 object ($m = 3$) in the whole range P_{des} . The temporal evolution of the density $\theta(t)$ for these two objects is shown in Fig. 1 when $P_{\text{des}} = 0.001$. We see that a smaller β leads to a slower and more gradual relaxation at early times and a longer tail at later times.

Symmetric objects, because of their uniform shape, can form close-packed structures during deposition. However, in reversible deposition, the ability of particles to desorb leads to various local configurations. This creates a heterogeneous relaxation process, where some regions of the system relax quickly (e.g., by filling voids), while others remain stable for longer periods. This leads to a distribution of relaxation timescales, as different particles or clusters experience different local environments (e.g., varying numbers of neighbors or binding sites). The presence of multiple relaxation pathways results in a stretched exponential relaxation, with a smaller β reflecting the broader distribution of timescales. In contrast, asymmetric objects, which have higher m values, can result in more disordered initial configurations, characterized by fewer equivalent states due to their lack of symmetry. Relaxation in such systems may involve fewer cooperative rearrangements, potentially leading to larger β (closer to 1).

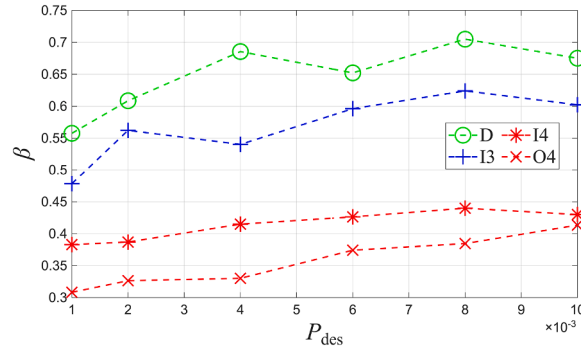


Fig. 9. Parameter β of the stretched exponential fit (Eq. (1)) vs desorption probability P_{des} for lattice animals D, I3, I4, and O4 with the same number of possible orientations $m = 3$, but various size (see, Table 1).

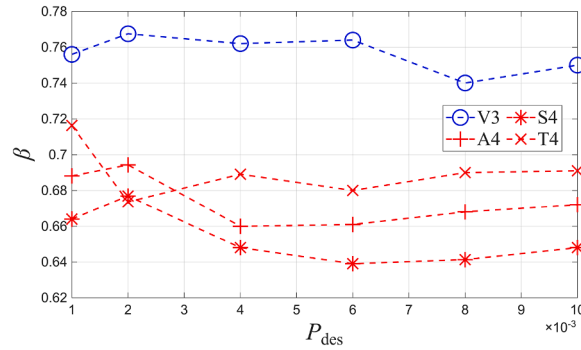


Fig. 10. Parameter β of the stretched exponential fit (Eq. (1)) vs desorption probability P_{des} for lattice animals V3, A4, S4, and T4 with the same number of possible orientations $m = 12$, but various size (see, Table 1).

The behavior of the density $\theta(t)$ near the jamming limit θ_j also confirms the influence of cooperative rearrangements of objects during the reversible deposition process. Figs. 1 and 2 illustrate that for small values of both m and P_{des} , density $\rho(t)$ does not fluctuate significantly near the jamming limit θ_j , and density evolution occurs over a much broader time scale. In other words, the smaller the values of m or P_{des} , the longer the system remains near the jamming limit. This dynamic behavior can be attributed to the competition between single-particle and multi-particle events. Single-particle events can bring the system to its jamming limit θ_j in a certain time t . If this time t is sufficiently short compared to the rate of two-particle transitions, the system will remain at $\theta(t) \approx \theta_j$ until two-particle events begin to influence the dynamics. This leads to a plateau in the time evolution of the density near the jamming limit. The duration of this plateau is determined by the values of m and P_{des} , since these parameters affect the transition rates for events involving two “well-placed” particles transitioning to one “not well-placed” particle, and vice versa [23,56]. It is clear that this relaxation behavior diminishes in the regime of strong desorption, where $P_{\text{des}} \rightarrow 1$, when the stretching exponent $\beta \rightarrow 1$.

Figs. 9 and 10 illustrate how the parameter β in the stretched exponential fit (Eq. (1)) depends on the desorption probability P_{des} for lattice animals with $m = 3$ and $m = 12$ possible orientations, respectively. The impact of object size n on the value of the fit parameter β is significant and consequently affects the dynamics of the reversible deposition process. For objects with the same number of possible orientations m , the exponent β tends to decrease as the object size increases. This reduction in the stretching exponent can be attributed to a rise in structural heterogeneity. Larger objects are more likely to form heterogeneous initial configurations during deposition. For example, they often create voids or defects in the deposited packing because they cannot effectively fill small gaps. During the reversible deposition process, these defects are filled or reorganized at different rates, depending on the local environment, such as the number of neighboring objects or the available free space. This structural heterogeneity and variability in the local relaxation dynamics give rise to a stretched exponential behavior of the density $\theta(t)$ with a lower value of β .

4. Conclusion

We have numerically investigated the kinetics of the lattice animal deposition process on a 3D cubic lattice in the presence of particle desorption. We focus on the time evolution of the density $\theta(t)$ in the whole post-jamming time range ($\theta(t) > \theta_j$). It was shown that the stretched exponential behavior (Eq. (1)) excellently describes the deposition dynamics well above the jamming limit. We have also emphasized the importance of multiparticle transitions in governing the late-time behavior of the density.

The influence of object symmetry on the relaxation time τ and the stretching exponent β in Eq. (1), which describes the approach of the system to equilibrium, was analyzed in detail. The characteristic time scale τ was found to decrease with the probability of

desorption P_{des} according to a power law relationship (9), $\tau = A (P_{\text{des}})^{-\gamma}$. The exponent γ remains unchanged in all shapes of the same size, while the parameter A changes depending on the number of possible orientations m of the shape. Our findings indicate that the deposition dynamics slows significantly as m decreases. Indeed, greater symmetry enhances the probability of single-particle readsorptions, which do not change the total number of deposited objects on the grid, leading to a slowdown in density growth above the jamming density. Furthermore, as the size n of the object decreases, the relaxation time τ changes to lower values for a given desorption probability P_{des} . This trend suggests that the deposition dynamics become faster with decreasing object size as a result of a reduction in the frustration of spatial adsorption.

The fitting parameter β in Eq. (1) characterizes the shape of the relaxation function and reflects the complexity or heterogeneity of the relaxation process. It has been confirmed that a lower value of β results in a slower and more gradual relaxation during the early stages, as well as a longer tail in the later stages. Furthermore, for objects of the same size, the value of β increases with the number of possible orientations m of the object. This finding highlights the significant role that the geometric characteristics and symmetry properties of extended objects play in the reversible RSA dynamics.

The adsorption-desorption model is frequently used by various authors to qualitatively represent the densification kinetics and other characteristics of weakly vibrated granular materials [11,12,28]. This model explains the density relaxation of a specific layer of granular material when subjected to a perpendicular tapping force. During a tapping event, particles randomly leave the layer (desorption events). Compaction occurs when particles fall back into the layer due to the influence of gravity (adsorption events). The ratio of desorption to adsorption probability, $P_{\text{des}}/P_{\text{a}}$, within the model plays a role similar to that of the intensity of vibration in real experiments. It is important to note that the dynamics of the reversible RSA model depends on excluded volume and geometrical frustration, just as in the case of granular compaction. Various laws have been proposed to describe how the packing fraction of a granular material increases with the number of taps [57]. Bideau et al. [58,59] have experimentally demonstrated that the dynamics of compaction is consistent with the stretched exponential law (1).

It has been observed that analogies can be drawn between the characteristic time of vibrational compaction of grains with different material properties and the parameter τ in the model of reversible deposition of 3D objects. Through this analogy, the symmetry properties of the extended objects in the RSA model are linked to the dissipative properties of the grains during vibratory compaction [27]. Indeed, multi-particle events in the reversible RSA model drive density growth above the jamming limit. Higher shape symmetry increases the chance of single-particle readsorption, which means more time between multi-particle events and slower densification. In real granular materials, increasing the coefficient of normal restitution (inelasticity parameter) in a shake cycle mainly speeds up energy loss. For very dissipative grains, the system is likely to stop quickly in a dilute state. As a result, less dissipative grains reach a higher packing fraction under the same number of taps, while more dissipative grains form arches that leave more empty space. In this way, the reversible RSA model on a 3D lattice captures the slow relaxation and compaction dynamics seen in real granular systems.

The three-dimensional lattice model presented in this work can be improved in order to study the compaction process in polydisperse granular systems under vibratory excitation. It is important to emphasize that dissipative properties of real granular particles would be included in our model through the symmetry properties of shapes.

Declaration of generative AI and AI-assisted technologies in the writing process

During the preparation of this work, the authors used Writefull in order to improve readability and refine the language and grammar of this manuscript. After using this tool/service, the authors reviewed and edited the content as needed and take full responsibility for the content of the published article.

CRediT authorship contribution statement

Julija R. Šćepanović: Writing – original draft, Validation, Methodology, Formal analysis; **Danica Stojiljković:** Writing – review & editing, Visualization, Software, Data curation; **Zorica M. Jakšić:** Writing – review & editing, Supervision; **Ljuba Budinski-Petković:** Writing – review & editing, Supervision; **Slobodan B. Vrhovac:** Writing – review & editing, Writing – original draft, Supervision, Project administration, Methodology, Investigation, Conceptualization.

Declaration of competing interest

The authors declare that they have no known competing financial interests or personal relationships that could have appeared to influence the work reported in this paper.

Acknowledgements

This work was supported by the Ministry of Science, Technological Development and Innovation of the Republic of Serbia. Numerical computations were performed on the PARADOX-IV supercomputing facility at the Scientific Computing Laboratory, National Center of Excellence for the Study of Complex Systems, Institute of Physics Belgrade.

References

- [1] T. Aste, Variations around disordered close packing, *J. Phys.: Condens. Matter* 17 (2005) 2361.
- [2] S. Torquato, F.H. Stillinger, Jammed hard-particle packings: from Kepler to Bernal and beyond, *Rev. Mod. Phys.* 82 (2010) 2633.
- [3] S. Torquato, Y. Jiao, Organizing principles for dense packings of nonspherical hard particles: not all shapes are created equal, *Phys. Rev. E* 86 (2012) 011102.
- [4] J.D. Bernal, The structure of liquids, *Proc. R. Soc. London Ser. A* 280 (1962) 299. Mathematical and Physical Sciences.
- [5] S. Torquato, Random Heterogeneous Materials: Microstructure and Macroscopic Properties, Vol. 16 of *Interdisciplinary Applied Mathematics*, Springer-Verlag, New York, 2002.
- [6] P.M. Chaikin, T.C. Lubensky, Principles of Condensed Matter Physics, Vol. 1, Cambridge University Press, New York, 2000.
- [7] T. Yamaguchi, T. Asada, H. Hayashi, N. Nakamura, Dependence of the packing structure of mesogenic groups on the flexible spacer length of liquid-crystalline side-chain polymers, *Macromolecules* 22 (1989) 1141.
- [8] J. Liang, K.A. Dill, Are proteins well-packed?, *Biophys. J.* 81 (2001) 751.
- [9] P.K. Purohit, J. Kondev, R. Phillips, Mechanics of dna packaging in viruses, *Proc. Natl. Acad. Sci.* 100 (2003) 3173.
- [10] J.W. Evans, Random and cooperative sequential adsorption, *Rev. Mod. Phys.* 65 (1993) 1281.
- [11] J. Talbot, G. Tarjus, P. Viot, Adsorption-desorption model and its application to vibrated granular materials, *Phys. Rev. E* 61 (2000) 5429.
- [12] L. Budinski-Petković, S.B. Vrhovac, Memory effects in vibrated granular systems: response properties in the generalized random sequential adsorption model, *Eur. Phys. J. E* 16 (2005) 89.
- [13] C. Zuppa, M. Ciacera, G. Zgrablich, Cooperative sequential adsorption of k -mers on heterogeneous substrates, *Langmuir* 15 (1999) 5984.
- [14] Z. Adamczyk, J. Barbasz, M. Zembala, Particle assembly on surface features (Patterned surfaces), *Langmuir* 23 (2007) 5557.
- [15] D. Stojiljković, J.R. Šćepanović, S.B. Vrhovac, N.M. Švrakić, Structural properties of particle deposits at heterogeneous surfaces, *J. Stat. Mech.* (2015) P06032.
- [16] J. Talbot, G. Tarjus, P.V. Tassel, P. Viot, From car parking to protein adsorption: an overview of sequential adsorption processes, *Colloids Surf. A* 165 (2000) 287.
- [17] L. Anton-Sanchez, C. Bielza, A. Merchán-Pérez, J.-R. Rodríguez, J. Defelipe, P. Larranaga, Three-dimensional distribution of cortical synapses: a replicated point pattern-based analysis, *Front. Neuroanat.* 8 (2014) 85.
- [18] G. Zhang, S. Torquato, Precise algorithm to generate random sequential addition of hard hyperspheres at saturation, *Phys. Rev. E* 88 (2013) 053312.
- [19] S. Torquato, T.M. Truskett, P.G. Debenedetti, Is random close packing of spheres well defined?, *Phys. Rev. Lett.* 84 (2000) 2064.
- [20] T. Bertrand, R.P. Behringer, B. Chakraborty, C.S. O'hern, M.D. Shattuck, Protocol dependence of the jamming transition, *Phys. Rev. E* 93 (2016) 012901.
- [21] J.J. Ramsden, G.I. Bachmanova, A.I. Archakov, Kinetic evidence for protein clustering at a surface, *Phys. Rev. E* 50 (1994) 5072.
- [22] E. Frey, A. Vilfan, Anomalous relaxation kinetics of biological lattice-ligand binding models, *Chem. Phys.* 284 (2002) 287.
- [23] R.S. Ghaskadvi, M. Dennin, Reversible random sequential adsorption of dimers on a triangular lattice, *Phys. Rev. E* 61 (2000) 1232.
- [24] P.L. Krapivsky, E. Ben-Naim, Collective properties of adsorption-desorption processes, *J. Chem. Phys.* 100 (1994) 6778.
- [25] L. Budinski-Petković, M. Petković, Z.M. Jakšić, S.B. Vrhovac, Symmetry effects in reversible random sequential adsorption on a triangular lattice, *Phys. Rev. E* 72 (2005) 046118.
- [26] I. Lončarević, L. Budinski-Petković, S.B. Vrhovac, A. Belić, Adsorption, desorption, and diffusion of k -mers on a one-dimensional lattice, *Phys. Rev. E* 80 (2009) 021115.
- [27] D. Arsenović, S.B. Vrhovac, Z.M. Jakšić, L. Budinski-Petković, A. Belić, Simulation study of granular compaction dynamics under vertical tapping, *Phys. Rev. E* 74 (2006) 061302.
- [28] G. Tarjus, P. Viot, Statistical mechanical description of the parking-lot model for vibrated granular materials, *Phys. Rev. E* 69 (2004) 011307.
- [29] I. Lončarević, L. Budinski-Petković, J.R. Šćepanović, Z.M. Jakšić, S.B. Vrhovac, Random sequential adsorption of lattice animals on a three-dimensional cubic lattice, *Phys. Rev. E* 101 (2020) 012119.
- [30] M. Beljin-Čavić, I. Lončarević, Lj. Budinski-Petković, Z.M. Jakšić, S.B. Vrhovac, Simulation study of random sequential deposition of binary mixtures of lattice animals on a three-dimensional cubic lattice, *J. Stat. Mech.* (2022) 053206.
- [31] M. Beljin-Čavić, Lj. Budinski-Petković, I. Lončarević, Z.M. Jakšić, S.B. Vrhovac, Random sequential adsorption of polydisperse mixtures on a cubic lattice, *J. Stat. Mech.* (2025) 013204.
- [32] D. Stojiljković, J. Šćepanović, Z. Jakšić, L. Budinski-Petković, S. Vrhovac, Percolation in random sequential adsorption of lattice animals on a three-dimensional cubic lattice, *Chin. J. Phys.* 90 (2024) 853.
- [33] D.W. Cooper, Random-sequential-packing simulations in three dimensions for spheres, *Phys. Rev. A* 38 (1988) 522.
- [34] J. Talbot, P. Schaaf, G. Tarjus, Random sequential addition of hard spheres, *Mol. Phys.* 72 (1991) 1397.
- [35] S. Torquato, O.U. Uche, F.H. Stillinger, Random sequential addition of hard spheres in high euclidean dimensions, *Phys. Rev. E* 74 (2006) 061308.
- [36] J.D. Sherwood, Packing of spheroids in three-dimensional space by random sequential addition, *J. Phys. A Math. Gen.* 30 (1997) 839.
- [37] M. Cieřla, Properties of random sequential adsorption of generalized dimers, *Phys. Rev. E* 89 (2014) 042404.
- [38] M. Cieřla, P. Kubala, Random sequential adsorption of cubes, *J. Chem. Phys.* 148 (2018) 024501.
- [39] M. Cieřla, P. Kubala, Random sequential adsorption of cuboids, *J. Chem. Phys.* 149 (2018) 194704.
- [40] W.F. Lunnon, Counting polyominoes, in: A.O.L. Atkin, B.J. Birch (Eds.), *Computers in Number Theory*, Academic Press, 1971, pp. 347–372.
- [41] W.F. Lunnon, Symmetry of cubical and general polyominoes, in: R.C. Read (Ed.), *Graph Theory and Computing*, Academic Press, 1972, pp. 101–108.
- [42] D.S. Gaunt, M.F. Sykes, H. Ruskin, Percolation processes in D-dimensions, *J. Phys. A Math. Gen.* 9 (1976) 1899.
- [43] G. Aleksandrowicz, G. Barequet, Counting polycubes without the dimensionality curse, *Discrete Math.* 309 (2009) 4576–4583.
- [44] I. Jensen, Enumerations of lattice animals and trees, *J. Stat. Phys.* 102 (2001) 865.
- [45] D.H. Redelmeier, Counting polyominoes: yet another attack, *Discrete Math.* 36 (1981) 191.
- [46] O.F. Inc, The On-Line Encyclopedia of Integer Sequences, 2019. Sequence A000162.
- [47] H. Goldstein, C. Pole, J. Safko, *Classical Mechanics*, 3, San Francisco, Addison Wesley, 2002. Rd ed.
- [48] J.W. Evans, D.R. Burgess, D.K. Hoffman, Irreversible random and cooperative processes on lattices: spatial correlations, *J. Math. Phys.* 25 (1984) 3051.
- [49] R.H. Swendsen, Dynamics of random sequential adsorption, *Phys. Rev. A* 24 (1981) 504.
- [50] E. Hinrichsen, J. Feder, T.J. ssang, Geometry of random sequential adsorption, *J. Stat. Phys.* 44 (1986) 793.
- [51] S. Manna, N.M. Švrakić, Random sequential adsorption: line segments on the square lattice, *J. Phys. A Math. Gen.* 24 (1991) 671.
- [52] J.C. Phillips, Stretched exponential relaxation in molecular and electronic glasses, *Rep. Prog. Phys.* 59 (1996) 1133.
- [53] J.C. Lagarias, J.A. Reeds, M.H. Wright, P.E. Wright, Convergence properties of the nelder-mead simplex method in low dimensions, *SIAM J. Optim.* 9 (1998) 112.
- [54] A.J. Kolan, E.R. Nowak, A.V. Tkachenko, Glassy behavior of the parking lot model, *Phys. Rev. E* 59 (1999) 3094.
- [55] W. Gilbert, W. Nicholson, *Modern Algebra with Applications*, Pure and Applied Mathematics: A Wiley Series of Texts, Monographs and Tracts, Wiley, 2004.
- [56] P. Ranjith, J.F. Marko, Filling of the one-dimensional lattice by k -mers proceeds via fast power-law-like kinetics, *Phys. Rev. E* 74 (2006) 041602.
- [57] G. Lumay, N. Vandewalle, Experimental study of the compaction dynamics for two-dimensional anisotropic granular materials, *Phys. Rev. E* 74 (2006) 021301.
- [58] P. Philippe, D. Bideau, Compaction dynamics of a granular medium under vertical tapping, *Europhys. Lett.* 60 (2002) 677.
- [59] P. Ribière, P. Richard, D. Bideau, R. Delannay, Experimental compaction of anisotropic granular media, *Eur. Phys. J. E* 16 (2005) 415.